Powder metallurgical production of 316L stainless steel/Niobium composites for Proton Exchange Membrane Electrolysis Cells (PEMECs)

N. F. Daudt[1*], F.J. Hackemüller[2], M. Bram[2],

[1]*Department of Mechanical Engineering, Technology Center, Universidade Federal de Santa Maria, 97105-900, Santa Maria, RS, Brazil*

[2]*Institute of Energy and Climate Research (IEK-1), Forschungszentrum Jülich GmbH, 52425, Jülich, Germany.*

**Corresponding author E-mail: natalia.daudt@ufsm.br*

Powder metallurgical production of 316L stainless steel/Niobium composites for Proton Exchange Membrane Electrolysis Cells (PEMECs)

Abstract

In this study, a composite made of a porous stainless steel (SS) 316L substrate coated with Nb was investigated as a novel porous transport layer (PTL) for Proton Exchange Membrane Electrolysis Cells (PEMECs). The fabrication of such SS316L/Nb composites using scalable and automatable powder metallurgical techniques as tape casting, screen-printing and field assisted sintering technology/spark plasma sintering (FAST/SPS) was described. Sintering behavior of the niobium layer and the interdiffusion at the SS316L/Nb interface were investigated by microstructural characterization. Powder metallurgical techniques such as screen-printing are the preferred method to achieve a porous Nb coating, while FAST/SPS is the preferred method for a better control of the SS316L/Nb interface by lowered interdiffusion. First electrochemical performance tests with SS316L/Nb composites demonstrate that they have the potential to replace the state-of-the-art titanium-based PTLs. The use of SS316L is expected to decrease manufacturing costs of PTLs, while the addition of niobium layer, due its excellent corrosion resistance in acid environment, aims to improve PEMECs lifetime and performance. Furthermore, Nb coatings on steel parts might even be attractive for biomedical implants, due to high biocompatibility of niobium.

Keywords: Niobium, 316L stainless steel, screen-printing, FAST/SPS, porous transport layer, PEM electrolysis

1. Introduction

Proton exchange membrane electrolysis cells (PEMECs) play a key role for the sustainable production of hydrogen and PEM electrolysis is suitable for coupling with wind and solar energy [1, 2]. Recently, several studies have been conducted on developing electrocatalyst and polymer electrolyte for PEMECs [3]. In comparison, there is relatively few researches focused on developing and improving porous transport layers (PTLs) for this kind of electrolysis cells. PTLs combine the function of transporting water, O_2 and H_2 molecules and electrons. Furthermore, they have to withstand pressures up to 50 bar if the system is operated in differential pressure mode. Due to high electrochemical overpotential, acidic environment and presence of oxygen in statu nascendi PTLs require materials with high corrosion resistance, good electrical conductivity and sufficient mechanical resistance to support the membrane [4]. Moreover, PTLs should have a high porosity degree, interconnected pores and homogenous pore distribution to enable water reaching effectively the catalytic side [3]. According to Ojong et al. [5] decreasing PTL thickness to 500 μm or less enables to

improve water transport to the membrane, being the basis of improved PEMEC performance. On the other hand, the results obtained by Borgardt et al. [6] and Hackemüller et al. [7] showed that 30% of porosity and thickness of 300–500 μm respectively are the best compromise for PTL made of sintered porous Ti tapes for combining low flow resistance and sufficient mechanical stability. Hackemüller et al. [7] proved that tape-casting technology is suitable for production of Ti tapes up to 470 x 470 mm^2 with 300 μm thickness, which make them suitable for application as PTLs of industrial electrolyzers.

Currently, Ti is the state of art PTLs due its great corrosion resistance and high ratio mechanical resistance/density [3, 4, 8]. However, use of titanium-based materials is one of the main causes of high costs of PEMECs. Furthermore, Ti-based PTLs are responsible for polarization losses by ohmic drop due to resistance against mass and current flow throughout its structure. Especially formation of passivating titanium oxide layer decreases electrical conductivity and durability of PTLs. Stainless steel is an alternative to lower material and manufacturing costs. Nevertheless, stainless steel has limited corrosion resistance in the harsh environment conditions of a PEMEC near to the electrochemically active water electrode. Dissolution of alloying elements might lead to poisoning of membrane and catalyst [9]. Therefore, stainless steel needs a corrosion resistant coating layer, such as niobium, for long-term operation under these conditions [10].

Recently, literature reports on niobium use in electrochemical devices due to its superior corrosion resistance and stability in acid environment. For instance, Weil et al. [11] and Hong and Weil [12] developed a niobium clad stainless steel (SS) bipolar plate for PEMFCs. Niobium was proven a suitable clad material for increasing performance of these bipolar plates. Niobium properties were excellent under the specific test conditions (acidic environment) and there was no weight loss found due to the formation of a very stable oxide on the niobium surface [13]. Feng et al. [14] tested a SS316L steel, which was implanted with niobium ions, as bipolar plate material for a PEMFC stack. Their results showed that niobium implantation could significantly improve corrosion resistance and electrical conductivity of SS316L in the simulated PEMFC environments. Lettenmeier at al. [10] investigated coatings based on Ti and Nb as efficient strategy to improve corrosion resistance of bipolar plates made of SS316L for PEMECs. Niobium coatings decreased contact resistance by almost one order magnitude, making niobium a promising alternative to platinum-based coatings with respect to reducing production costs [10].

In this context, coating stainless steel with protective niobium layer appears as a promising approach to produce cost effective PTL and replace Ti as state-of-the-art PTLs. In its metallic state, niobium has a lower ohmic resistance (15.2 μΩ.cm [15]) compared to Ti (42 μΩ.cm [16]). In ambient atmosphere both titanium and niobium tend to passivate, i.e. they form a very stable nm-thick oxide on the surface. For the PEMEC application, it is remarkable that the niobium oxides have a higher conductivity than titanium oxides, e.g. of Nb_2O_5 is ca. 10^{-4} $S \cdot cm^{-1}$ [15], while TiO_2 is ca. 10^{-6} $S \cdot cm^{-1}$ [17]. In spite of the niobium excellent properties and its potential for application as structural parts or coatings for electrochemical and biomedical devices, there are very few literature reports about

suitable processing of Nb, especially if porous structures are the aim. A specific method of processing niobium is powder metallurgy (PM), which enables wide spread possibilities regarding net-shape manufacturing of complex parts with high material utilization, adjustment of functional porosity and deposition as functional coatings, like PTLs for PEMECs [10, 13].

In the present study, the potential of manufacturing a PTL based on a porous stainless steel substrate covered by a porous niobium layer was investigated. To best of our knowledge, this specific kind of porous 316L/Nb composites completely processed by a scalable and automatable powder metallurgical technologies, has not been described in literature before. The main difference of this application to Nb coated bipolar plates as e.g. described by Lettenmaier et al. [10] is the direct contact of the porous Nb layer to the electrode, where the water splitting takes place. At this position in the PEMEC stack, the requirements for long-term stable operation of the composite are different from the requirements of bipolar plates. The challenges for manufacturing SS316L/Nb composites are the mismatch in thermal expansion coefficient of niobium (8.2 $x10^{-6}$ m/m·K at 800 K) and SS316L (19.5 $x10^{-6}$ m/m·K at 800 K) and the mismatch in melting temperatures of Nb (2469 ºC) and SS316L (1400 ºC). Furthermore, the interdiffusion at the interface is expected to influence electrochemical performance. Therefore, PTLs made of SS316L/Nb composites were manufactured using established powder metallurgy route (combination of tape casting and screen-printing) with subsequent sintering. Both tape casting and screen-printing have already been proven to be suitable for large-scale and cost-effective production of ceramic structures [18]. For proof of concept, electrochemical function of this novel PTL was successfully demonstrated in a single cell test on laboratory scale. For better control of interdiffusion at the interface, preliminary Field Assisted Sintering Technology/Spark Plasma Sintering (FAST/SPS) experiments were performed.

2. Experimental

2.1. Starting materials

Spherical stainless steel 316L powder (Sandvik Osprey Powders, Germany) and niobium powders with acicular particle shape (HC Starck, Germany) were used as starting powders (Figure 1). Particle size distribution of starting powder were measured in-house and are shown in Table 1.

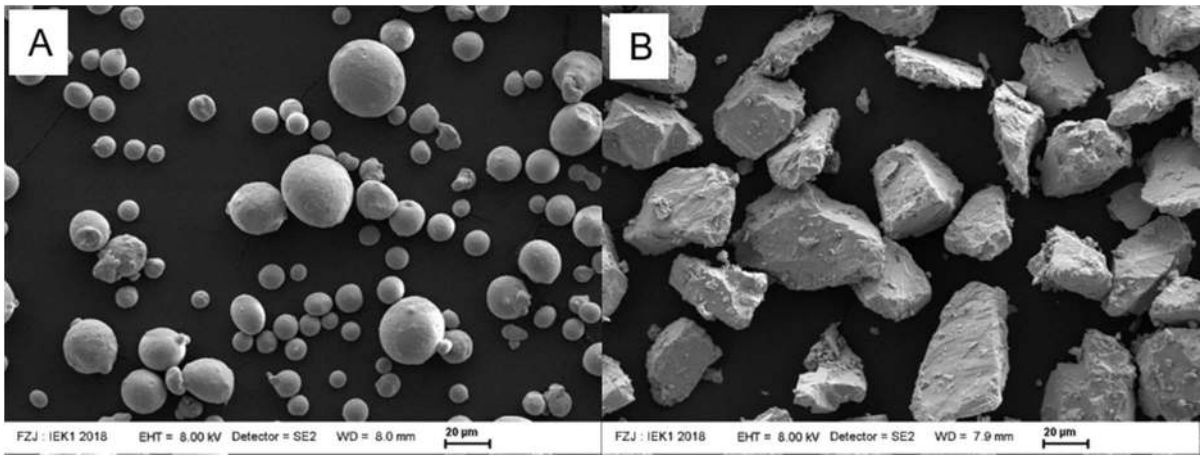

Figure 1. SEM of precursor powders: (a) SS316L powder and (b) Nb powder.

Table 1. Particle size distribution and interstitial content of the starting powders.

Sample	**Particle size distribution**		
	D_{10} [µm]	**D_{50} [µm]**	**D_{90} [µm]**
SS 316L powde	11.7	18.6	29.0
Niobium powder	23.8	40.6	58.2

2.2. Manufacturing SS316L substrates by tape casting

SS316L substrates of 70 x 70 mm^2 and 260 µm thickness were produced by tape casting using an automated tape casting line (FGA500, SAMA, Germany). The position of doctor blade was adjusted to achieve a thickness of the tapes of ca. 350 µm in the not-sintered state. The casting speed was 250 mm/min. For final shaping, the tapes were cut to a size of 70 x 70 mm^2. A detailed description of the tape casting process of PTLs can be found elsewhere [19, 7]. Thermal debinding and sintering were performed in a vacuum furnace (Type 121212 WM, Thermal Technology GmbH, Bayreuth, Germany). Prior to sintering SS316L tapes were heated up to 500 ºC at 2 K/min under argon flow, where the temperature was held for 30 min to remove the binder. Afterwards, samples were heated under vacuum (< 10^{-3}Pa) up to 1100 ºC at 5 K/min followed by a dwell time of 180 min at sintering temperature.

2.3. Screen-printing of Nb layer

Composite structures were produced by screen-printing of a Nb layer on tape casted SS316L substrate. For that, a Nb slurry was prepared by mixing Nb powder with a Terpineol and ethylcellulose based solution. The slurry was printed using semi-automatic screen printer (EKRA, Germany). Nb layers of 40 x 40 mm^2 and 60 x 60 mm^2 were printed on green and sintered SS316L tapes. After

printing, the samples were placed in a drying oven at 50 ºC for 180 min to remove the solvents. Then, samples were heated up with 5 K/min under vacuum (< 10^{-3}Pa) to the co-sintering temperature, which was varied in the range of 850°C – 1150°C. In all cases, a dwell time of 180 min was used. Co-sintering was performed in a vacuum furnace already mentioned before. Manufacturing parameters of SS316L/Nb composites are summarized in Table 2. A sample code was set to describe samples: SS316L stands for 316L stainless steel, "g" for samples, where printing was done on green tapes, "s" for samples, where printing was done on sintered tapes, Nb for niobium and digits for the co-sintering temperature.

Table 2. Manufacturing parameters of SS316L/Nb composites.

Sample code	Pre-sintering temperature of SS316L tapes	Co-sintering temperature
SS 316L1100	1100 ºC	-
SS 316Lg_Nb850	-	850 ºC
SS 316Lg_Nb1000	-	1000 ºC
SS 316Lg_Nb1100	-	1100 ºC
SS 316Ls_Nb1100	1100 ºC	1100 ºC
SS 316Lg_Nb1150	-	1150 ºC
SS 316Ls_Nb1150	1100 ºC	1150 ºC

2.4. Manufacturing SS316L/Nb composites by FAST/SPS

SS316L/Nb composites were produced by FAST/SPS aiming to study the controlled interdiffusion at the interface. At this stage of development, production of almost dense layers was preferred, since a more clearly defined SS316L/Nb interface was achieved. A sharp interface eases to study the interdiffusion depth. FAST/SPS process was carried out using a lab-scale device (FCY-HPD5, FCT Systeme GmbH, Germany) with standard graphite tool of 20 mm inner diameter. First, the Nb layer was consolidated. For that, 12 g of Nb powder were poured into the graphite die and pre-compacted by uniaxial pressure of 50 MPa for 60 s. A graphite foil was previously placed between powder and punches as well as between powder and die. Firstly, the Nb layer was sintered by FAST/SPS under vacuum (ca. 3Pa) at 1500 °C. The heating rate was 100 ºC/min and the dwell time at sintering temperature was 30 s. A uniaxial pressure of 50 MPa was applied during the whole thermal cycle. After sintering, the carbide layer formed at the Nb surface due to the contact to graphite foils was removed by mechanical grinding.

The Nb disks sintered by FAST/SPS were placed back into the graphite die and 9 g of SS316L powder was poured into the die. Again, a graphite foil was placed in between powder and tool parts. Nb disks and SS316L powders were pre-compacted using a uniaxial pressure of 50 MPa for 60 s. Then, the SS316L/Nb composites were sintered by FAST/SPS under vacuum (ca. 3Pa) at 1000 °C. Again, a heating rate of 100 ºC/min was used and the temperature was held for 20 s. The same uniaxial

pressure of 50 MPa was applied during the whole thermal cycle. Dwell time at 1000°C was chosen as short as possible to achieve a good adherence at the interface while reducing interdiffusion to a minimum. After sintering, the carbide layer formed at the SS316L and Nb surface was removed by mechanical grinding.

2.5. Sample Characterization

The SS316L/Nb composites were characterized by X-Ray Diffraction (XRD), using Brag-Brentano geometry (θ-2θ) in a Bruker D4 X-Ray Diffractometer (Bruker GmbH, Germany). XRD patterns were taken on the substrate side (sample bottom), on the top surface (niobium layer) and at the interface of the SS316L/Nb samples in order to analyze interdiffusion and sample composition. Microstructural characterization of the cross-section of polished samples was performed by using tabletop scanning electron microscope (TM3030, Hitachi High Technology, Japan) and a scanning electron microscope (JSM 6360, Jeol Inc, USA). Sample thickness was measured by using a micrometer screw (Multytoyo, Japan). Thickness of Nb layer as well as sample porosity were measured by image analysis of several SEM images of the cross-sections, using ImageJ software. Chemical composition was analyzed by Energy-dispersive X-Ray Spectroscopy (EDS) using a Quantax 75 (Bruker Nano GmbH, Germany) device accomplished to Hitachi microscopy. Several EDS measures were performed on determined regions of the samples and mean values of chemical composition were calculated. Sample surfaces were characterized using a Cyber Scan CT300 optical profilometer (Cyber Technologies, Eching-Dietersheim, Germany). The uptake of interstitial elements was measured by chemical analysis using IR spectroscopy (LECOTCH/CS600).

Sintered parts were evaluated by electrochemical measurements in order to analyze the potential of porous SS316L/Nb composites for application as PTLs of PEMECs. For that, samples were cut by laser into 42 x 42 cm pieces and mounted on the anode side of a single test cell ring. The standard membrane electrode assembly (MEA) for PEM electrolysis at Forschungszentrum Jülich was used. More details on the experimental setup can be found in literature [19, 7]. Nafion membrane (E300 with Nafion® 117, Greenerity GmbH, Germany) was used as electrolyte. The anode side was fed with a water volume of 25 ml/min. Polarization curves were obtained at 80 ºC, with steps of 2 A/cm^2 and 5 min dwell time per measuring point, up to a voltage of 2.2 V. Established PTLs made of sintered porous Ti tapes (ca. 300 µm thickness and 44 % porosity) were used as reference samples (Figure 2). The tape casted Ti-PTLs were produced as described elsewhere [19, 7]. The sintering was carried out at 900 °C with a dwell time of 120 min.

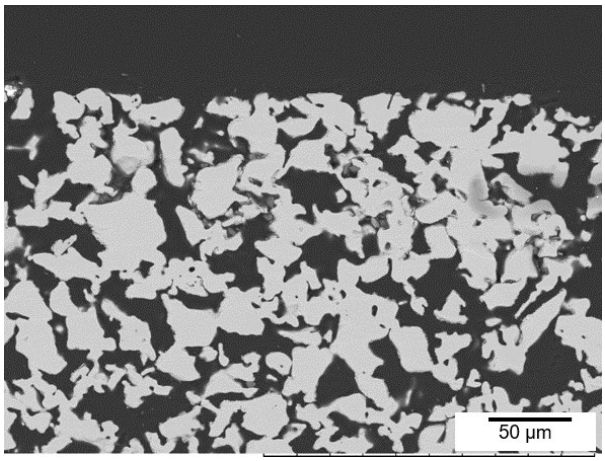

Figure 2. SEM image of Ti-PTL used as reference samples.

3. Results

3.1 Screen-printing Nb layer on SS 316L tapes

Table 3. Sample composition measured by EDS in the different regions (indicated in Figure 3) of S316L/Nb composites produced by printing Nb powders on green SS316L tapes.

Sample	Region	Nb (wt.%)	Fe (wt.%)	Cr (wt.%)	Ni (wt.%)	Mo (wt.%)	Mn (wt.%)
SS316Lg_ Nb850	A1	0.1 ± 0.08	69.8 ± 0.7	16.5 ± 0.3	9.97 ± 0.6	2.4 ± 0.24	1.3 ± 0.35
	A2	0.1 ± 0.07	70.1 ± 0.2	14.0 ± 4.0	9.84 ± 0.7	2.4 ± 0.24	1.1 ± 0.18
SS316Lg_ Nb1100	D1	96.9 ± 1.2	0.4 ± 0.5	0.1 ± 0.1	0.1 ± 0.08	2.5 ± 0.4	0.1 ± 0.17
	D2	0.1 ± 0.08	70.0 ± 0.7	17.4 ± 0.6	9.7 ± 0.4	2.4 ± 0.4	0.4 ± 0.4
	D3	0.0 ± 0.0	70.9 ± 1.1	17.0 ± 0.3	9.2 ± 0.9	2.7 ± 0.1	0.1 ± 0.1
SS316Lg_ Nb1150	E1	97.0 ± 1.1	0.6 ± 0.5	0.2 ± 0.3	0.1 ± 0.3	1.93 ± 0.6	0.1 ± 0.2
	E2	0.8 ± 0.35	69.2 ± 0.5	16.0 ± 0.5	10.8 ± 0.9	2.86 ± 0.4	0.3 ± 0.2
	E3	0.2 ± 0.25	69.3 ± 0.2	16.5 ± 0.3	10.7 ± 0.45	2.54 ± 0.5	0.8 ± 0.37

At first, a sintering study was conducted on samples, which were produced by screen-printing a Nb layer on green 316L tapes followed by co-sintering at different temperatures. With respect of processing costs, co-sintering is preferred compared to multiple sintering steps. As expected, sintering was improved with increasing temperature and porosity was decreased (Figure 3). Samples sintered at 850 ºC showed a very poor sintering behavior and as consequence remained very brittle, while for samples sintered at 1100 and 1150 ºC porosity and brittleness could be significantly decreased. In parallel, Nb, Mn, Fe, Cr and Ni interdiffusion increased as a function of temperature (Table 3) and distribution of these elements was found all over samples cross-section, especially for samples sintered

at 1100 and 1150 ºC. Sintering neck formation on Nb particles was mainly observed at the direct contacts between SS316L and Nb particles. At highest sintering temperature, a thicker Nb layer was obtained. This result can be explained by on avoiding flaking of weakly sintered particles at this temperature (Table 4).

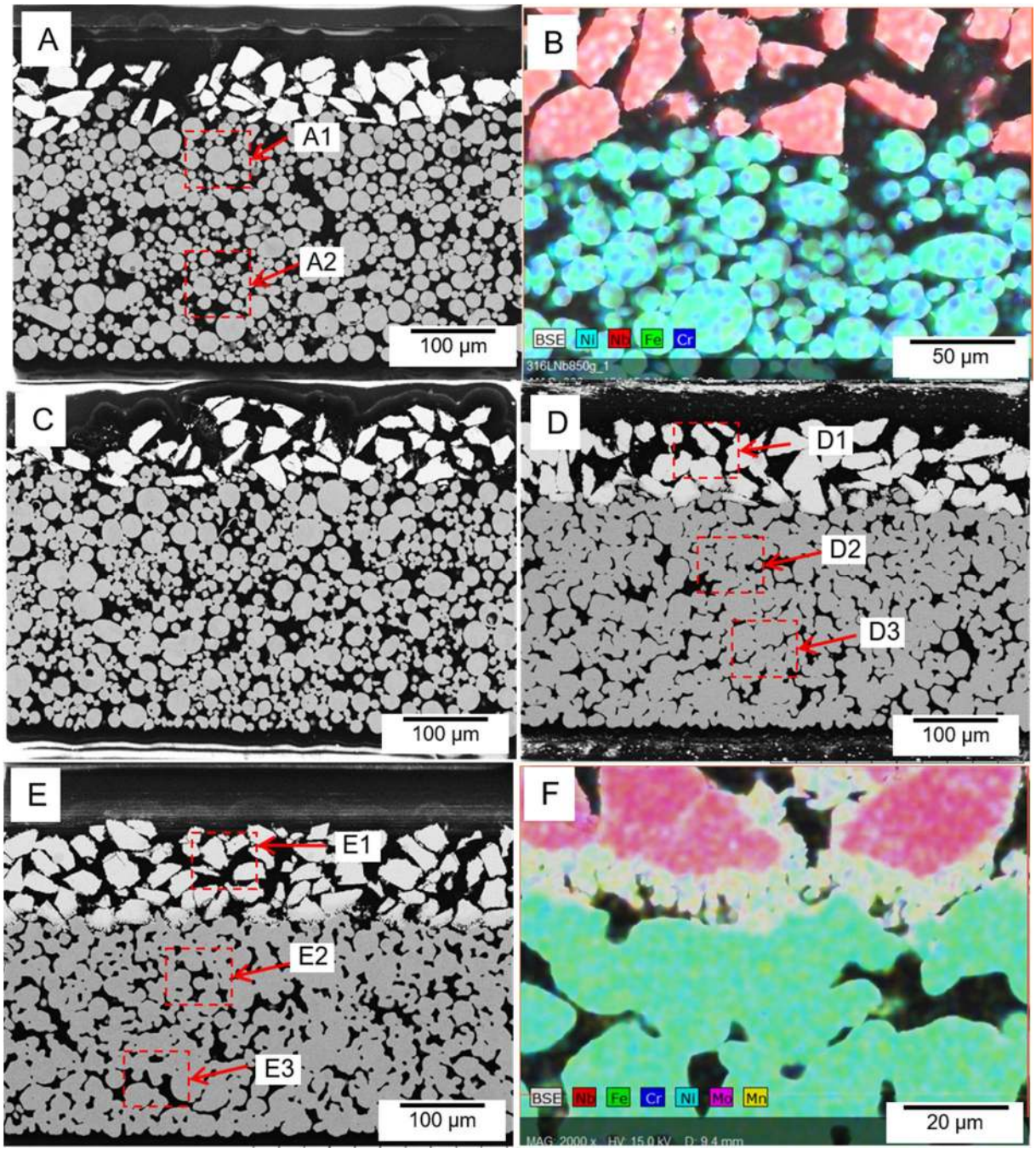

Figure 3. SEM images and EDS mapping of SS316L/Nb composites produced by printing Nb powders on green SS316L tapes and sintering at: (a, b) 850 ºC, (c) 1000 ºC, (d) 1100 ºC and (e, f) 1150 ºC.

Table 4. Thickness and shrinkage of SS316L/Nb composites.

Sample	Thickness of Nb layer	Total Thickness	Shrinkage in thickness	Porosity of SS316L substrate (Vol.%)
SS316Lg_Nb850	57 µm	353 ± 16 µm	6 µm	35.3 ± 0.1
SS316Lg_Nb1000	70 µm	366 ± 30 µm	- 5 µm	33.1 ± 0.4
SS316Lg_Nb1100	87 µm	356 ± 8 µm	44 µm	22.8 ± 6.3
SS316Lg_Nb1150	100 µm	351 ± 7 µm	55 µm	20.6 ± 0.5
SS316Ls_Nb1100	46 µm	333 ± 10 µm	101 µm	21.4 ± 0.8
SS316Ls_Nb1150	112 µm	369 ± 22 µm	60 µm	16.2 ± 1.4

Intermetallic compounds were formed at the SS316L/Nb interface of samples sintered at higher temperature such as 1100 and 1150 ºC (Figure 4). The formation of intermetallic compounds is mainly restricted to this interface. Once, intermetallic compounds were not observed in XRD pattern of sample substrate or surface, but only in the interface region (Figure 4). Furthermore, there was a precipitation of niobium carbide in the Nb layer, which is probably related to residual carbon from the binder. With respect to the phase diagram, niobium carbide precipitation is expected even for very low concentration of carbon (≤ 0.01 wt.%) [20]. Sintering temperatures above 1100 ºC resulted in bending of samples, which is caused by the mismatch in the sintering temperature and shrinkage of SS316L and Nb.

In order to decrease surface bending during sintering, samples were produced from printing Nb layer on pre-sintered SS316L substrates and then again co-sintered at 1100 and 1150 ºC. As expected, printing on pre-sintered tapes resulted in reduced bending and shrinkage of SS316L substrate when compared to samples produced from Nb printing on green tapes (Table 4). However, a decreased adherence of the Nb layer was found. The microstructure (Figure 5) and interdiffusion values (Table 5) were similar to the ones found for Nb printed on green tapes (Figure 3 and Table 3). Samples sintered at 1150 ºC had a higher interdiffusion and decreased flaking; therefore, a thicker Nb layer was obtained. On the other hand, the bending on SS316Ls_Nb1150 samples was higher than on SS316Ls_Nb1100 samples, which can be related to lower porosity. Figure 6 shows a convex bending of the S316L/Nb composites in direction of the Nb layer, which was in the range of 0.2 – 0.3 mm in the case of samples sintered at 1100 °C and around 0.5 mm in the samples sintered at 1150 °C. This bending is mainly caused by two reasons: i.) The strong difference of the sintering temperatures between 316L and Nb leads to more pronounced shrinkage of the 316L layer at a given sintering temperature ii.) The bending effect is aggravated by the mismatch of thermal expansion. Higher thermal expansion coefficient of 316L is coupled with a stronger contraction when cooling from sintering temperature. Similar effects are described in literature when sintering composites with layered structure like solid oxide fuel cells [21]. Controlled plastic deformation can be applied for

flattening the S316L/Nb composites and it will be investigated in our ongoing study. Nevertheless, the EC-values (Figure 7) prove that there is contact in the cells even if this bending appears.

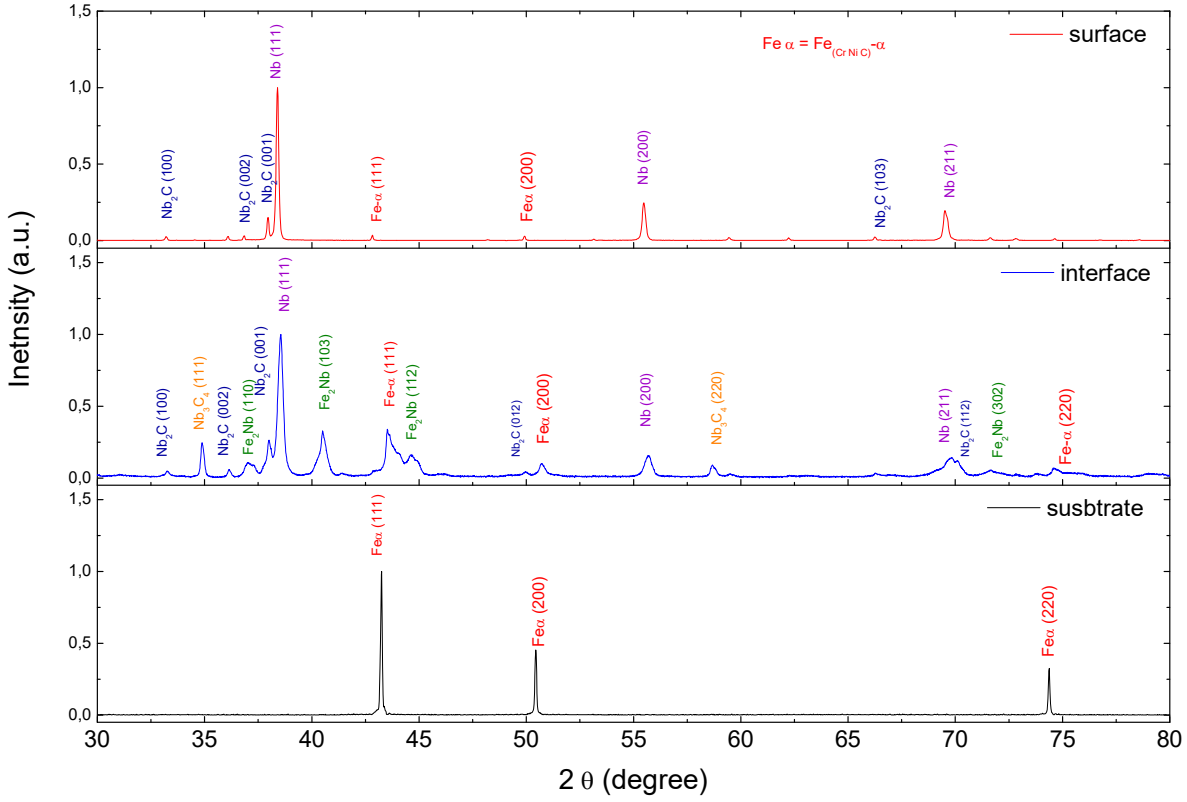

Figure 4. X-Ray pattern of SS316Lg_Nb1100 sample obtained on sample surface, interface and substrate (bottom).

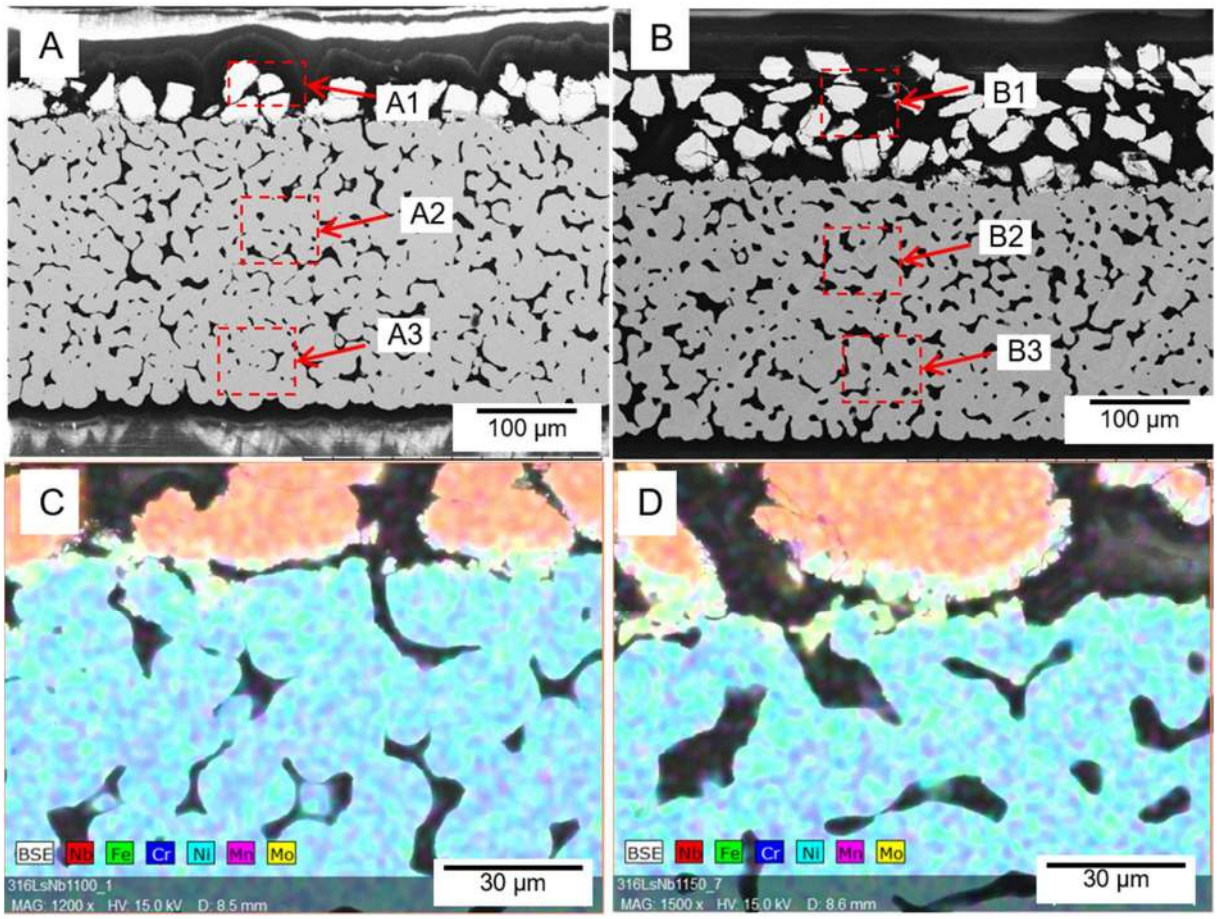

Figure 5. SEM images and EDS mapping of SS316L/Nb composites produced by printing Nb powders on pre-sintered SS316L tapes, subsequently co-sintered at: (a,c) 1100 ºC and (b,d) 1150 ºC.

Table 5. Sample composition measured by EDS in the different regions (indicated in Figure 5) of SS316L/Nb composites produced by printing Nb powders on sintered SS316L tapes.

Sample	Region	Nb (wt.%)	Fe (wt.%)	Cr (wt.%)	Ni (wt.%)	Mo (wt.%)	Mn (wt.%)
SS316Ls_ Nb1100	A1	96.3 ± 1.3	1.0 ± 0.8	0.2 ± 0.17	0.1 ± 0.1	2.2 ± 0.69	0.2 ± 0.19
	A2	0.2 ± 0.16	70.7 ± 0.7	16.5 ± 0.8	10.0 ± 0.4	2.5 ± 0.1	0.2 ± 0.1
	A3	0.1 ± 0.17	70.6 ± 0.6	15.8 ± 1.1	10.9 ± 1.2	2.4 ± 0.38	0.1 ± 0.1
SS316Ls_ Nb1150	B1	96.7 ± 1.7	0.6 ± 0.6	0.3 ± 0.3	0.14 ± 0.19	2.2 ± 1.4	0.1 ± 0.09
	B2	0.4 ± 0.2	70.6 ± 0.3	16.8± 0.7	9.2 ± 0.1	2.8.± 0.1	0.2 ± 0.06
	B3	0.1 ± 0.17	70.6 ± 0.9	15.9 ± 0.9	10.8 ± 1.5	2.4 ± 0.4	0.3 ± 0.3

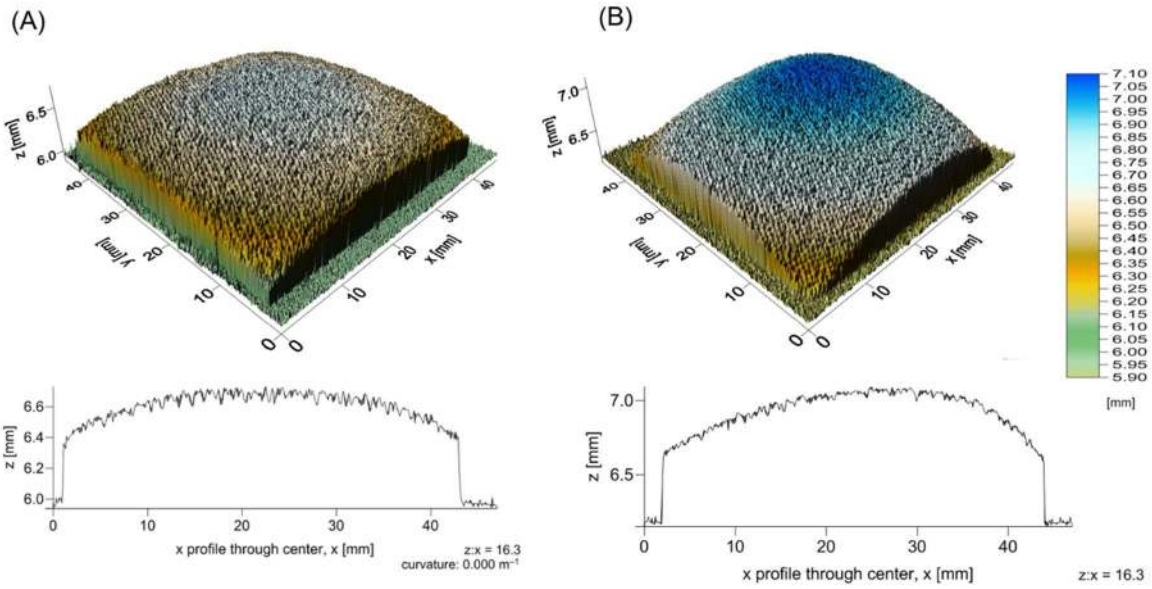

Figure 6. Topography of (a) SS316Ls_Nb1100, and (b) SS316Ls_Nb1150.

Table 6. Interstitial content of the starting powders and sintered samples before and after electrochemical tests.

Sample	Interstitial content		
	O (wt.%)	N (wt.%)	C (wt.%)
SS 316L powder	0.057 ± 0.001	0.176 ± 0.001	0.02 ± 0.002
Niobium powder	0.176 ± 0.001	< 0.0045	< 0.0008
SS316Ls_Nb1100_sintered	0.058 ± 0.014	< 0.0008	0.026 ± 0.002
SS316Ls_Nb1100 after electrochemical test	0.076 ± 0.007	0.0013 ± 0.0001	0.011 ± 0.004
SS316Ls_Nb1150_sintered	0.069 ± 0.007	0.011 ± 0.0004	0.015 ± 0.001
SS316Ls_Nb1150 after electrochemical test	0.083 ± 0.012	0.009 ± 0.0005	0.013 ± 0.001

An interstitial content of 0.058 ± 0.014 wt.% oxygen, 0.0013 ± 0.0001 wt.% nitrogen and 0.011 ± 0.004 wt.% carbon was found in the case of sample SS316Ls_Nb_1100 and 0.069 ± 0.007 wt.% oxygen, 0.011 ± 0.0004 wt.% nitrogen and 0.015 ± 0.001 wt.% carbon in the case of sample SS316Ls_Nb_1150 (Table 6). The interstitial content slightly increased with sintering temperature; however, it remains close to SS316L starting powder, indicating that the interstitial uptake during sintering was almost negligible. After electrochemical testing, further increase of oxygen content to 0.076 ± 0.007 wt.% and 0.083 ± 0.012 wt.% on SS316Ls_Nb_1100 and SS316Ls_Nb_1150 samples respectively was found. It is assumed that this uptake does not influence the electrochemical performance significantly, but further tests including conductivity measurement and surface sensitive

analysis (e.g. XPS in combination with high resolution SEM [22] are required to come to a sound conclusion.

Electrochemical tests

Electrochemical performance of SS316L/Nb composites and Ti standard PTLs (Figure 7) were similar at current densities below 1 A/cm^2, which indicates SS316L/Nb composites have the potential to be applied as PTLs of PEM electrolysis cells. At higher current densities, there was an increased overpotential in the SS316L/Nb composites when compared to reference Ti-PTLs. The increased overpotential in SS316L/Nb structure are probably related to the lower porosity compared to reference samples and the flaking of Nb particles, which can enter in between the surface pores and, thereby, impede the water transport through the pores. By optimizing porosity, particle size of the Nb coating and the layer adherence the contact between catalytic layer and PTL can be improved as well as the mass transport, so that the increase of cell voltage can be avoided. Furthermore, during PEMEC operation, both niobium and titanium will form oxide layers at the surface. Once niobium oxide has higher conductivity than titanium oxide, a higher performance for PEMEC is expected by further enhancing microstructure of SS316L/Nb composites. Anyway, these primary results are promising regarding the potential for PTL of PEMEC application and further studies are planned to improve the microstructure and to investigate the long-term stability of the composites under operation conditions.

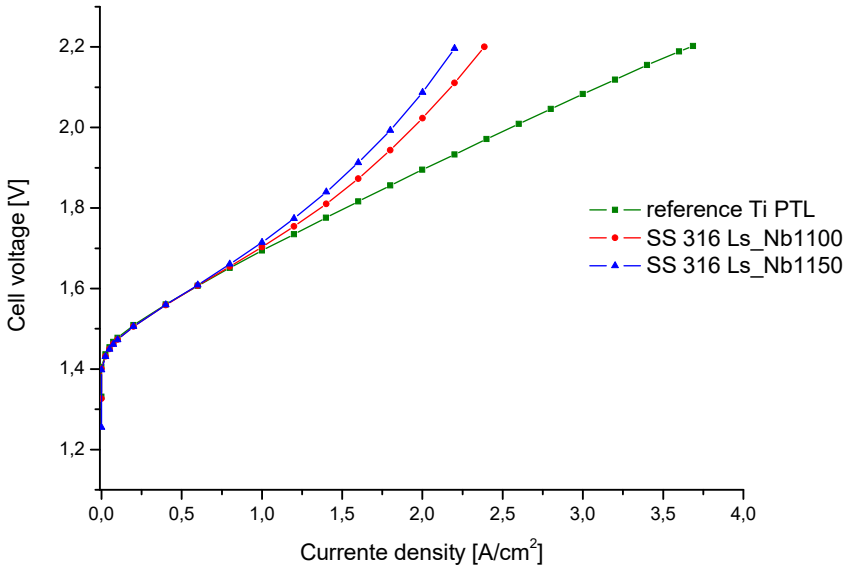

Figure 7. Polarization curves of reference Ti PTL and SS316Ls_Nb110 and SS316Ls_Nb1150 composites.

3.2. FAST/SPS production of SS316L/Nb composites structure

A preliminary study was conducted to estimate the potential of FAST/SPS to produce SS316L/Nb composites. The advantages of FAST/SPS compared to conventional, pressure less co-firing of 316L/Nb composites are: i.) It is expected that FAST/SPS enables co-sintering of both materials at relatively low temperatures and short dwell times. This reduces the interdiffusion depth and the risk of secondary phase formation at the interface. Furthermore, occurrence of Joule heating at the contact points between Nb particles is expected to support the formation of stable sintering necks. ii.) Concave shaping of FAST/SPS tools might be an effective measure to level the convex bending caused by mismatch of sintering activity and thermal expansion coefficient.

In a first approach, the potential of FAST/SPS to clearly reduce interdiffusion and second phase formation was investigated. For achieving a well-defined interface, it was decided to do this experiment by using an almost dense Nb sample, which was pre-sintered by FAST/SPS at 1500°C. Then, 316L powder was poured in the die and sintered at 1000°C with a dwell time of 20 s and a pressure of 50 MPa. A good adhesion between both materials was achieved (Figure 8). The very short sintering times lead to clearly reduced interdiffusion between Nb and SS316L layers (Table 7) and the effect was mainly concentrated on the interface zone between both materials. Under given conditions, formation of a very thin diffusion layer, with a thickness of a few 100 nm was found and only few Nb atoms diffused in the SS316L layer (Figure 8 c). This low interdiffusion rate contributes to reliably avoid formation of intermetallic phase, such that neither intermetallic phase, nor carbides were observed in the XRD pattern (Figure 9). Avoiding carbide formation is required to ensure enough ductility and minimize sample embrittlement. FAST/SPS is a promising route for producing SS316L/Nb composites, once it allows an improved sintering of Nb particles at lower temperature (1500 ºC), when compared to the 1800 - 2000 ºC applied for sintering Nb in resistive furnace [23]. By using lower sintering temperature or applying a suitable pore former material, FAST/SPS can become a suitable technique for production of porous composite structures as well. The results of this preliminary experiment are the basis of our ongoing work aiming on to produce 316L/Nb composite PTLs by FAST/SPS and to conduct related electrochemical tests.

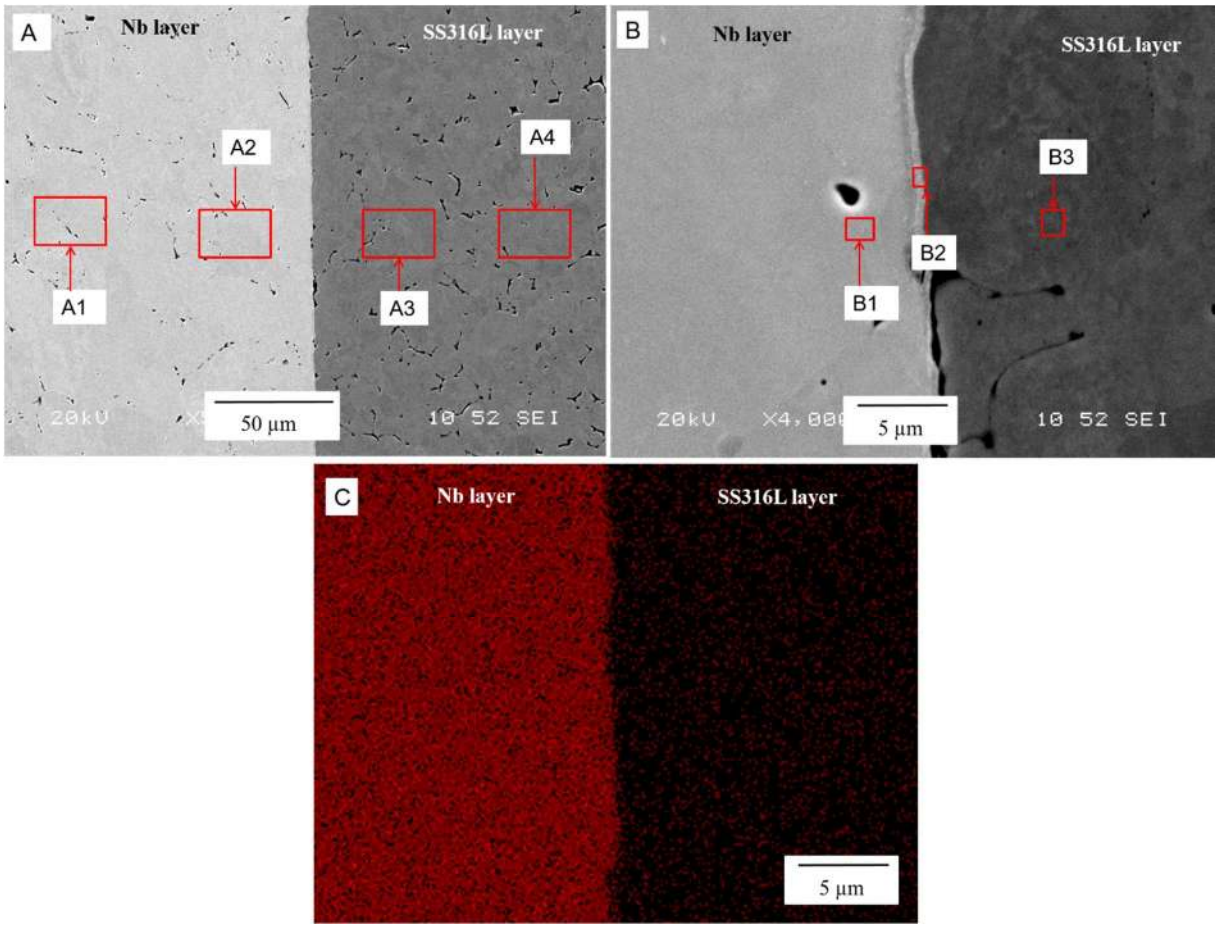

Figure 8. (a, b) SEM images of the cross-section of SS316L/Nb composite produced by FAST/SPS. Nb layer was consolidated at 1500 ºC and SS316L layer at 1000 ºC. (c) EDS mapping of Nb.

Table 7. Sample composition measured by EDS of regions indicated on SEM image of SS316L/Nb composite produced by FAST/SPS (Figure 8).

Point	Nb (wt.%)	Fe (wt.%)	Cr (wt.%)	Ni (wt.%)	Mo (wt.%)	Mn (wt.%)
A1	97.7	0.10	0.08	0.03	1.95	0.16
A2	97.5	0.03	0.01	0.06	2.38	0.00
A3	0.34	69.4	16.2	10.4	2.53	1.11
A4	0.22	70.9	17.2	8.53	2.18	0.98
B1	96.1	1.76	0.43	0.00	1.76	0.00
B2	71.0	17.9	4.21	2.25	4.63	0.00
B3	2.81	67.0	15.8	9.98	2.78	1.62

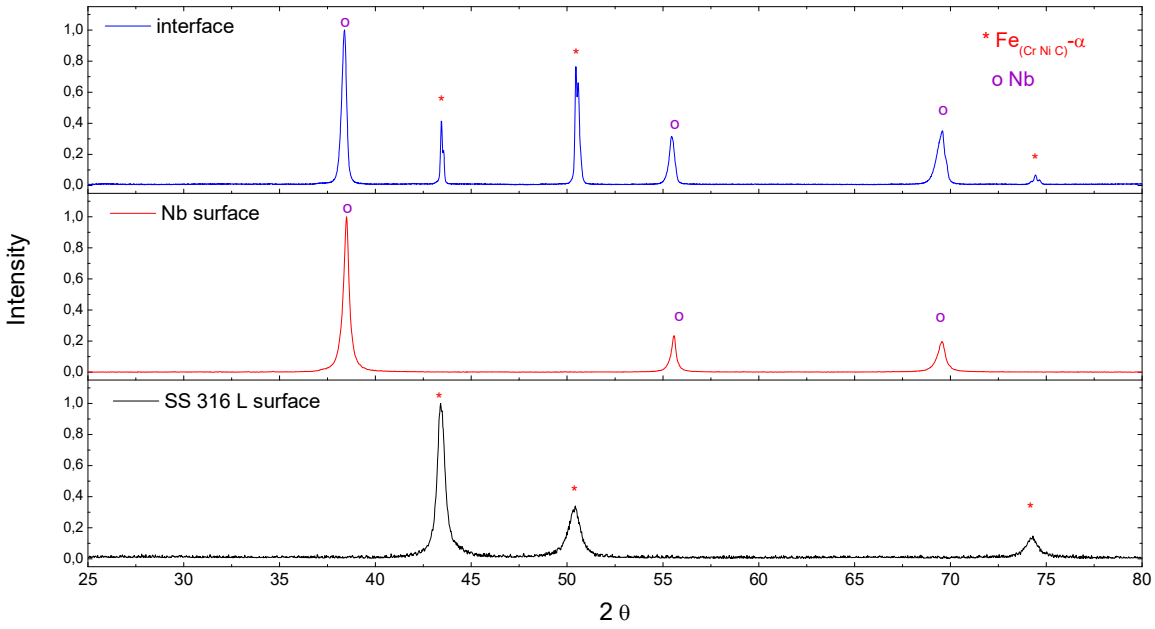

Figure 9. X-Ray pattern of SS316L/Nb composite produced by FAST/SPS.

4. Conclusions and summary

Screen-printing of Nb layer on both green and pre-sintered tapes was proved to be suitable technique for manufacturing SS316L/Nb composites, which have the potential to be used as porous transport layers (PTLs) for PEMEC electrolyzers. PTLs with thickness varying between 350 and 370 µm were produced. This thickness is in the range reported in the literature as suitable for application as PTLs in PEMECs. Varying sintering temperatures in the range of 850 to 1150 ºC were investigated. As expected, higher sintering temperature increased the interdiffusion at the interface SS316L/Nb, nonetheless resulting in an improved sintering of Nb particles. In addition, higher sintering temperatures led to an increased bending of the samples, caused by deviating sintering shrinkage rates and thermal expansion coefficients of both materials. Screen-printing a Nb layer on pre-sintered SS316L considerably decreased sample bending during co-sintering. So that, the best compromise between higher adhesion layer and lower bending seems to be on samples produced from printing a Nb layer on sintered tapes and final sintering at 1150ºC (SS316Ls_Nb1150 samples). Regarding its electrochemical performance, the novel SS316L/Nb PTLs behave similar to the standard Ti PTLs up to a current density of 1 A/cm^2. However, at higher current densities indication of a mass transport limitation was observed. By tailoring Nb particle size and its sintering behavior, a higher electrochemical performance is expected. The results obtained so far prove that SS316L/Nb composites are a candidate for PTLs application, nevertheless further microstructure optimization is

still required. Furthermore, it is expected that SS316L/Nb composites might also have a potential for biomedical implants due to excellent corrosion properties

As alternative production route, FAST/SPS is expected to be suitable for manufacturing of SS316L/Nb PTLs. Preliminary experiments reveal improved sintering of Nb particles and a better control of interdiffusion at interface SS316L/Nb. However, this technique still requires efforts to adapt the processing to allow production of thinner layers, porous structures and samples of larger size.

Acknowledgments

Financial support from the Brazilian funding agency FAPEGRS is acknowledged. The authors are also grateful for the experimental support of Werner Herzhof and Denise Günther from the Institute of Energy and Climate Research, Forschungszentrum Jülich GmbH as well as of Angelica D. Schneider from Laboratório de Magnetismo e Materiais Magnéticos, Universidade Federal de Santa Maria.

Disclosure statement

No potential conflict of interest was reported by the authors.

References

[1] R. E. Clarke et al., "Direct coupling of an electrolyser to a solar PV system for generating hydrogen," *International Journal of Hydrogen Energy,* vol. 34, pp. 2531-2542, 2009.

[2] B. Paul, J. Andrews, "Optimal coupling of PV arrays to PEM electrolysers in solar–hydrogen systems for remote area power supply," *International Journal of Hydrogen Energy,* vol. 33, pp. 490-498, 2008.

[3] M. Carmo, D.L. Fritz, J. Mergel, D. Stolten, "A comprehensive review on PEM water electrolysis," *International journal of hydrogen energy,* vol. 38, pp. 4901-4934, 2013.

[4] S.A. Grigoriev, V.I. Porembsky,V.N. Fateev, "Pure hydrogen production by PEM electrolysis for hydrogen energy," *Int J Hydrogen Energy,* vol. 31, p. 171–175, 2006.

[5] E.T. Ojong, J.T.H. Kwan, A. Nouri-Khorasani, A. Bonakdarpour, D.P. Wilkinson, T. Smolinka, "Development of an experimentally validated semiempirical fully-coupled performance model of a PEM electrolysis cell with a 3-D structured porous transport layer," *Int J Hydrogen Energy,* vol. 42, pp. 25831-25847, 2017.

[6] E. Borgardt, O. Panchenko, F. J. Hackemüller, J. Giffina, M. Bram, M. Müller, W. Lehnert, D. Stolten, "Mechanical characterization and durability of sintered porous transport layers for polymer electrolyte membrane electrolysis," *Journal of Power Sources,* vol. 374, pp. 84-91, 2018.

[7] F. J. Hackemüller, E. Borgardt, O. Panchenko, M. Müller, M. Bram, "Manufacturing of Large-Scale Titanium-Based Porous Manufacturing of Large-Scale Titanium-Based Porous Electrolysis by Tape Casting," *Adv. Eng. Mater. ,* vol. 1801201, 2019.

[8] G. Chen, G.Z. Li, C.S. Xiang, S.Y. Zhao, P. Tan, H.P. Tang, P. Cao, "Characterisation and properties of powder rolled porous Ti sheets and IrO2/Ti electrodes," *Powder Metallurgy,* vol. 59, p. 249 – 255, 2016.

[9] M. Langemann,D. Fritz, M. Müller, D. Stolten, "Validation and characterization of suitable materials for bipolar plates in PEM water electrolysis," *Int J Hydrogen Energy,* vol. 40, pp. 11385-11391, 2015.

[10] P. Lettenmeier, et. al., "Low-Cost and Durable Bipolar Plates for Proton Exchange Membrane Electrolyzers," *Scientific Reports,* vol. 7, p. 44035, 2017.

[11] K.S. Weil, G. Xia, Z. G. Yang, J. Y. Kim, "Development of a niobium clad PEM fuel cell bipolar plate material," *International Journal of Hydrogen Energy,* vol. 32, p. 3724– 3733, 2007.

[12] S.T. Hong, K.S. Weil, "Niobium-clad 304L stainless steel PEMFC bipolar plate material," *Journal of Power Sources,* vol. 168, pp. 408-417, 2007.

[13] S. Lædre, O.E. Kongstein, A. Oedegaard, "Materials for Proton Exchange Membrane water for Proton Exchange Membrane water," *nternational Journal of Hydrogen Materials,* vol. 42, pp. 2713-2723, 2017.

[14] K. Feng, Z. Li, X. Cai, P.K. Chu, "Corrosion behavior and electrical conductivity of niobium implanted 316L stainless," *Surface & Coatings Technology,* vol. 205, pp. 85-91, 2010.

[15] C. Nico, T. Monteiro, M.P.F. Graça , "Niobium oxides and niobates physical properties: Review and prospects," *Progress in Materials Science,* vol. 80, pp. 1-37, 2016.

[16] Annual Book of ASTM Standards (Volume 02.04: Non-ferrous Metals), West Conshohocken, PA, USA: ASTM International, 2006.

[17] T. Ioroi, H. Kageyama, T. Akita, K. Yasuda, "Formation of electro-conductive titanium oxide fine particles by pulsed UV laser irradiation," *Physical Chemestry Chemical Physics,* vol. 12, p. 7529–7535, 2010.

[18] F. Tietz, H.P. Buchkremer, D. Stöver, "Components manufacturing for solid oxide fuel cell," *Solid State Ionics,* Vols. 373-381, pp. 152-153, 2002.

[19] F.J. Hackemüller, M. Bram, E. Borgadt, O. Panchenko, "Porous titanium current collectors for water electrolysis made by tape casting," in *European annual powder metallurgy congress and exhibition*, Milan, Italy, 2017.

[20] J.F. Smith, O.N. Carlson, R.R. De Avillez, "The niobium carbon system," *J Nuclear Materials,* vol. 148, no. 1, pp. 1-16, 1987.

[21] W. Bao, Q. Chang, G. Meng, , "Effect of NiO/YSZ compositions on the co-sintering process of anode-supported fuel cell," *J. Membr. Sci.,* vol. 259, no. 1-2, pp. 103-109, 2005.

[22] E. Hryha, R. Shvab, M. Bram, M. Bitzer, L. Nyborg, "Surface chemical state of Ti powders and its alloys: Effect of storage conditions and alloy composition," *Appl. Surf. Sci.,* vol. 388, p. 294–303, 2016.

[23] G. Aggarwal, I. Smid S.J. Park, R.M. German, "Development of niobium powder injection molding. Part II: Debinding and sintering," *International Journal of Refractory Metals & Hard Materials,* vol. 25, p. 226–236, 2007.